J Low Temp Phys (2009) 157: 36–56
DOI 10.1007/s10909-009-9930-y

Current-Temperature Diagram of Resistive States in Long Superconducting $YBa_2Cu_3O_7$ Strips

K. Harrabi · F.-R. Ladan · Vu Dinh Lam · J.-P. Maneval · J.-F. Hamet · J.-C. Villégier · R.W. Bland

Received: 26 March 2009 / Accepted: 27 July 2009 / Published online: 12 September 2009

Abstract Using a sequence of stepped bias currents in the nanosecond range, we have studied the destruction of superconductivity in *c*-axis textured $YBa_2Cu_3O_7$ strips of various thickness and structure (single or multi-layers). Sufficiently far from T_c, vortex flow fades out and gradually gives way to localized dissipative structures, which can be interpreted either as Phase-Slip Centers (PSC) or normal Hot Spots (HS). A plot of the corresponding threshold currents in the current–temperature (I–T) plane indicates when each of them will occur, and how to switch over from one to the other, in a manner similar to that demonstrated for metallic materials (cf. Ladan et al., J. Low Temp. Phys. 153:103, 2008). The capability of some YBCO strips to support PSC's at arbitrarily low temperatures escapes the common picture.

Keywords High-T_c films · Phase-Slip Centers · Critical currents · Phonon escape

PACS 74.76.Bz · 61.72.Mm · 74.40.+k · 74.50.+r

K. Harrabi · F.-R. Ladan · V.D. Lam · J.-P. Maneval (✉)
Laboratoire Pierre Aigrain de l'École Normale Supérieure, Associated with CNRS (UMR 8551), Université Paris 6, and Université Paris 7, 24 rue Lhomond, 75231 Paris 5, France
e-mail: maneval@lpa.ens.fr

J.-F. Hamet
CRISMAT-ENSICAEN (UMR-CNRS 6508), Bd du Maréchal Juin, 14050 Caen 4, France

J.-C. Villégier
CEA-INAC-SPSMS, 17 Avenue des Martyrs, 38054 Grenoble 9, France

R.W. Bland
Department of Physics and Astronomy, SFSU, San Francisco, CA 94132, USA

1 Introduction: Current-Induced Resistive States in Narrow Strips

If a diameter smaller than the coherence length ξ is the primary criterion [1, 2], high-T_c superconducting wires are poor candidates for demonstrating one-dimensional (1-D) transport. However, the observation of current-induced voltage jumps, sensitive to microwave irradiation, in the current–voltage (I–V) characteristics of constrictions of ceramic $YBa_2Cu_3O_7$ (YBCO) has been interpreted in terms of phase-slip centers (PSC) [3]. In addition, it has been established [4] that strips wider than the Ginzburg-Landau (G-L) coherence length ξ can support PSCs, or more properly phase-slip lines, provided the electron inelastic relaxation time substantially exceeds the coherence time τ_0. In narrow epitaxial YBCO strips the dissipation was found to shift from vortex flow (VF) near the critical temperature T_c to resistive singularities characteristic of 1-D transport, namely PSCs, and hot spots (HS) at lower temperatures [5]. The purpose of this paper is to organize the variety of states arising in a single YBCO strip as a function of temperature and current $\{T, I\}$, in analogy to the study recently devoted in this journal to niobium strips [6].

While HSs are merely normal zones maintained above the critical temperature T_c by the Joule effect, for a current larger than a well-defined threshold value I_h, a PSC is a particular dissipative state of a 1-D filament traversed by a current larger than the depairing G-L critical current I_c. In what may be called the standard PSC model [1], it consists of a localized dissipation unit, centered on a core of size ξ and extending on both sides over the quasiparticle diffusion length Λ (typically 1 μm). Therefore, an ideal current-controlled I–V isotherm appears as a tilted staircase, with a series of equal vertical steps, each one corresponding to the nucleation of a new PSC. The inclined parts of each step, of dynamic resistance $R_u = dV/dI$, extrapolate to a common intersection I_S with the $V = 0$ axis, where I_S represents the time-averaged PSC superfluid current. If the current happens to exceed $I_h(T)$, the filament leaves the superconducting state, and the resistance takes on its full normal-state value. That ideal description needs in some cases to be adapted to the load line of the bias circuit.

Exciting a strip with current step-functions of the time offers several advantages, in addition to simply limiting the power dissipation. First of all, a delay time t_d, depending in a specific way upon the reduced current intensity I/I_c [5, 7], precedes the nucleation of a PSC. This statement applies to HS nucleation as well, if a HS necessarily follows the formation of a PSC, as is the case with niobium [6]. So, a sizeable delay (nanoseconds) between the application of a supercritical current step and the first voltage rise appears as an unmistakable signature of the nucleation of either a PSC or a HS singularity, which suffices to distinguish these modes from VF dissipation. Furthermore, under current-controlled drive (electrical source impedance $\gg$ load impedance), a HS constantly fed with $I > I_h(T)$ grows in length at a constant rate and so produces a linearly rising voltage, contrasting with the time independence of the PSC voltage response.

Which of these resistive modes is effective for given $\{T, I\}$ conditions can be pictured (Sect. 2) on a diagram of the critical currents $I_c(T)$ and $I_h(T)$. These two curves usually intersect at some temperature T^* with the property $I_c < I_h$ for $T > T^*$, and *vice versa*, which justifies the familiar statement [1, 2]: PSCs near T_c and HS at low temperature. By observing the temporal evolution, retarded or not, stable or

growing, of the voltage response (Sect. 4), an I–T diagram is constructed. At $T < T^*$, the first visible response to a single-step excitation is, as expected, a HS since $I_h < I_c$, but it only occurs at the higher current $I_c(T)$. The determination of I_h at $T < T^*$ therefore requires a contour in the I–T plane involving a two-step technique. By using a similar procedure, a HS state can be made to retreat, or even to make a transition to a PSC state, at temperatures where PSCs have not been supposed to exist (Sect. 5). In exceptional cases the special electronic properties of YBCO can lead to $I_c < I_h$ everywhere, thus allowing the formation of PSCs at all temperatures (Sect. 6). Table 1 summarizes the observations made with a number of different samples. Finally, an Appendix is devoted to the measurement of delay times and to their application in the determination of phonon escape times, which in turn can be used to compute film temperatures.

It is concluded that—phenomenologically—current-carrying epitaxial YBCO strips behave essentially like any other superconducting material, aside from the last distinction made just above.

2 I–T Diagram and Specific Properties of YBCO Films

The I–T diagram of resistive states amounts to a comparison between the G-L depairing current density $J_c(T)$ and the minimum current density $J_h(T)$ allowing the formation of a hot spot. Let us first define $J_u(T_b)$ as the density whose Joule dissipation per unit volume ρJ_u^2, where ρ is the normal state resistivity, is sufficient to maintain a uniformly heated strip in the normal state on a substrate at temperature T_b, so that

$$\rho J_u^2 = C\tau^{-1}(T_c - T_b) \tag{1}$$

with C standing for the volumetric specific heat near T_c. In YBCO films, the cooling, or bolometric, time τ, related to the more familiar thermal boundary resistivity R_{bd} by $\tau = R_{bd}Cb$, where b represents the film thickness, is to a large extent a temperature-independent quantity, as will be discussed later. For simplicity, we will also assume that the current density is uniform across a transverse section of the filament, and that the electron-phonon interactions are sufficiently rapid for a single temperature T to describe the state of the system at a given position along the strip. For large temperature deviations from T_c, C can no longer be considered as a constant. In this case it is more appropriate to replace the product $C(T_c - T_b)$ by the enthalpy difference $\Delta h(T_b \to T_c) = h(T_c) - h(T_b)$, where $h(T)$ is the definite integral of C from 0 K to temperature T

$$\rho J_u^2 = \tau^{-1}\Delta h(T_b \to T_c) \tag{1'}$$

However, in order to sustain a steady localized HS, the Joule effect per unit volume ρJ^2 must compensate not only for the heat loss to the thermal bath considered above, but also for the longitudinal heat conduction along the filament. The combination of these two modes of heat transfer requires for HS formation [6, 8] a minimum current density J_h given by

$$\rho J_h^2 = pC\tau^{-1}(T_c - T_b) \tag{2}$$

in the linear approximation of heat transfer. The numerical factor p is equal to 2 under the assumption of continuity of the heat conductivity across the HS borders. For large temperature deviations, as with (1′), we will replace (2) by

$$\rho J_{\mathrm{h}}^2 = p'\tau^{-1}\Delta h(T_{\mathrm{b}} \to T_{\mathrm{c}}) = p'\rho J_{\mathrm{u}}^2 \tag{2'}$$

with a numerical factor p' which might differ somewhat from p.

As an example, one could estimate the current density J_{h0} in the extreme case of an YBCO strip on a substrate cooled to $T_{\mathrm{b}} = 0$ K. Assuming $p' = 2$, $b = 100$ nm, $\rho = 100\ \mu\Omega$ cm, plus the relation $\tau/b = 75$ ps/nm established experimentally for YBCO films deposited on MgO [9], and $h(T_{\mathrm{c}}) = 45\ \mathrm{J\,cm^{-3}}$, derived from by integration of heat capacity data [10, 11], (2′) yields $J_{\mathrm{h0}} \approx 10\ \mathrm{MA/cm^2}$. (Frequent uses of this numerically defined $h(T)$ will appear in this work.) A similar calculation performed at 77 K would gives $J_{\mathrm{h}}(77\ \mathrm{K}) \sim 6\ \mathrm{MA/cm^2}$.

On the other hand, the effective critical current cannot be predicted *a priori* in $YBa_2Cu_3O_7$ devices. One could use for J_{c} the expression [12] $J_{\mathrm{c}} = h/2\pi\mu_0 e\lambda^2\xi$, in which h, μ_0, and e are respectively the Planck constant, the magnetic permeability of vacuum, and the electronic charge. But with $\xi \sim 1.5$ nm for the coherence length in the (a, b) YBCO plane, and $\lambda \sim 250$ nm for the London penetration depth at 77 K, J_{c} would approach $\sim 1\ \mathrm{GA/cm^2}$, an enormous density indeed. Although such values have been achieved in exceptionally narrow bridges [12], the percolative character of the superconducting conduction in wider c-axis oriented films limits the *average* current density J_{c}, defined as I_{c} divided by the filament cross section, to just a few $\mathrm{MA/cm^2}$. This value just happens to fall in the range of the thermal threshold current densities J_{h}, and that coincidence introduces situations not found in metallic superconductors.

In view of the preceding estimates of J_{h0} and J_{c0}, it is not clear which is larger, so that no general prediction can be drawn as to whether the $J_{\mathrm{h}}(T)$ and $J_{\mathrm{c}}(T)$ curves cross. Both cases, $J_{\mathrm{c0}} > J_{\mathrm{h0}}$ and J_{c0} (noted J'_{c0}) $< J_{\mathrm{h0}}$ are considered in Fig. 1a, but a study of the less usual second case will be delayed until Sect. 6. ($J_{\mathrm{c0}} < J_{\mathrm{h0}}$ is favored by a good thermal contact, or by a small critical current density, of whichever origin). A universal property of (1) is to imply a $(1-t)^{1/2}$-dependence for $J_{\mathrm{h}}(t)$ near T_{c}, becoming vertical at $T = T_{\mathrm{c}}$, in contrast with J_{c} which, as t approaches 1, has a form varying from $(1-t)^{3/2}$ to $(1-t)$, depending on the filament width [8]. (Here t is the reduced temperature T/T_{c}). This ensures that the inequality $J_{\mathrm{h}} > J_{\mathrm{c}}$ holds near T_{c} in all cases. Low-T_{c} strips or whiskers, as well as most high-T_{c} thin strips, have $J_{\mathrm{h0}} < J_{\mathrm{c0}}$. Therefore there must be an intersection at some crossing temperature T^* separating the high-T domain, where PSCs appear first (star in Fig. 1a) when increasing the current up to $J_{\mathrm{c}}(T_{\mathrm{b}})$, from the low-$T$ domain where $J_{\mathrm{h}} < J_{\mathrm{c}}$.

At bath temperature $T_{\mathrm{b}} < T^*$, the first curve to be met by currents of increasing intensity is $J_{\mathrm{h}}(T_{\mathrm{b}})$ at point L. Although that is theoretically the HS threshold, the filament experiences no loss of superconductivity at this level. For a voltage to appear, a transient PSC (fuzzy star in Fig. 1a), generated at a value $J \geq J_{\mathrm{c}}(T_{\mathrm{b}})$, is first required, a process that necessitates a delay time t_{d} [7], by analogy with the Nb filaments [6]. Only then is the excited PSC zone converted into the hot spot $\mathrm{HS}_<$ (the index $<$ is for $T_{\mathrm{b}} < T^*$), because the dissipation exceeds the limit imposed by (2) (or 2′). In brief, monitoring the first response to a single step-pulse of current probes $I_{\mathrm{c}}(T)$ at

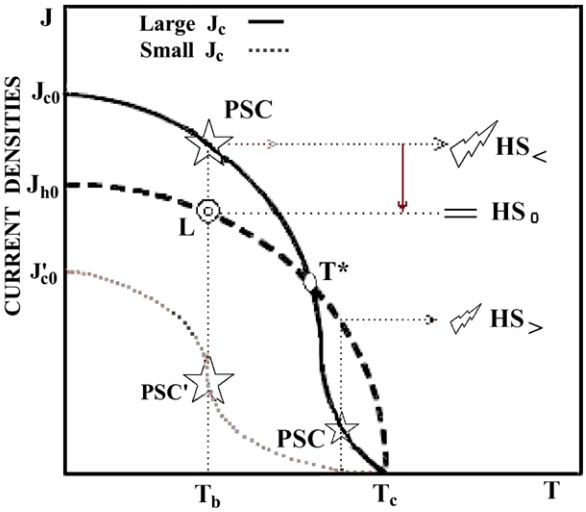

Fig. 1a (Color online) Principle of construction of the J–T diagram for 1-D resistive states. The first voltage response to a single current step appearing with a delay determines the graph $J_c(T)$. The branch $J_h(T_b)$ above T^* is obtained by an increase of the current. For $T_b < T^*$, the current density is first raised to $J' > J_c(T_b)$, then reduced until the voltage response is flat → HS threshold $J_h(T_b)$. The high-J_c and the (infrequent) low-J_c case end respectively at J_{c0} and J'_{c0} at $T = 0$ K. Stars are for PSCs (transient for $T_b < T^*$), rising arrows for HS

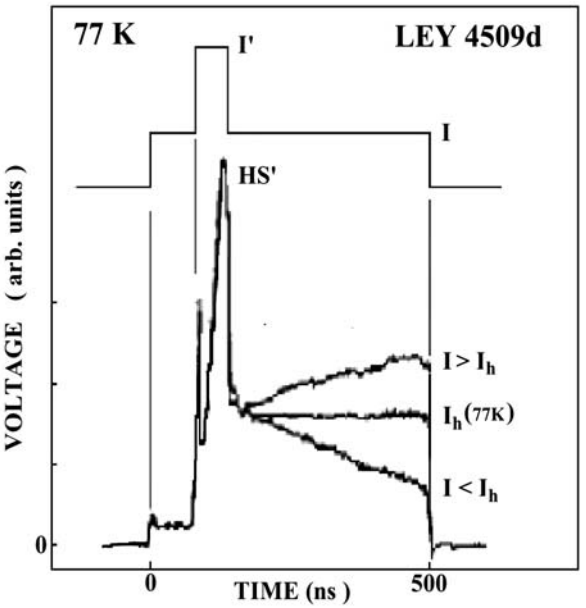

Fig. 1b Current temporal pattern (top) and voltage response in LEY4809d for three values (in mA) of the return current I: 97.75; I_h (maintaining a stationary voltage) = 97.35; and 74.45. Vertical scales adjusted so as to display three final responses originating from the same level

all temperatures from 0 K to T_c. Let us remark that, once a dissipative state has been created, the critical current becomes a function of the local film temperature T, as opposed to $I_h(T_b)$ which remains a function of the substrate temperature only.

Measuring $I_h(T_b)$ above T^* is straightforward: I_h is obtained by raising the current beyond $I_c(T_b)$, until the PSC flat voltage switches into a rising voltage revealing a hot spot $HS_>$. On the other hand, the low-temperature ($T_b < T^*$) branch requires a two-step procedure, still respecting the condition of controlled current bias. Thanks to a primary short pulse of intensity $I' > I_c(T_b)$, some part of the filament is first

launched into the HS' state, identified by its fast rising voltage (see oscilloscope traces in Fig. 1b), then subjected to a current of smaller intensity I. If this "return current" is above $I_h(T_b)$, an increasing voltage testifies to an expanding HS (top trace). However, for $I < I_h(T_b)$, a receding HS (lower trace) is observed. The current that maintains the steady level HS_0 should then correspond to $I_h(T_b)$ and so may be used to complete the (I_c, I_h, T) diagram. More complex behaviours, involving a return to PSC states, are detailed in Sect. 5. A pulsed laser excitation may also be substituted for the current pulse I' [6].

The length effective in the determination of the PSC differential resistance R_u is twice the quasi-particle diffusion length $\Lambda = v_F(\tau_c \tau_R/2)^{1/2}$, where τ_c is the elastic collision time, and τ_R is the transverse inelastic relaxation time [2]. For an order-of-magnitude evaluation, we will take a Fermi velocity $v_F \approx 2.2 \times 10^5$ m/s in the YBCO ab plane, and $\tau_c \approx 150 \exp(-T/12\ \mathrm{K})$ ps, following [13]. For τ_R, we will substitute the inelastic lifetime τ_{in} related to the microscopic processes of energy loss and of recombination, as found experimentally in YBCO [14]. Using these values one finds a temperature-dependent Λ, ranging from ~ 0.5 μm at 80 K, to about twenty times longer length at 60 K. Provided PCSs may be formed at low T, their measured length should reflect that exceptionally wide range.

Compared to metallic superconductors, YBCO is characterized by a low concentration of free charge carriers, and consequently a rather weak electronic contribution to the thermal conduction which is thus dominated by the lattice conduction. A thermal diffusivity of only $D_{th} = 3.3\ (\mu m)^2/\mu s$ at 77 K in the ab plane was found [11] for bulk samples of high crystalline quality. We assume comparable values to hold in epitaxial films. Consequently, small values are expected for the HS nominal growth velocity [6] $U_0 = \sqrt{D_{th}/\tau} \approx 15$ m/s, if one takes $\tau = 5$ ns as a typical figure for the film cooling time. Similarly, one would find about 0.15 μm for the thermal healing length, or a HS minimum half-length of, $\eta = \sqrt{D_{th}\tau}$.

3 Experimental Procedures and Samples

The YBCO samples reported on in this paper were deposited using a variety of techniques. Except in one case (LZCYB77:35 nm YBCO/70 nm YSZ/10 nm CeO_2/Silicon), the substrates were polished [100] MgO surfaces, in order to induce oriented growth of the film along the c-axis. YBCO films LEY 4553w and 4809d, from CRISMAT-Caen, were grown by laser ablation ($\lambda = 248$ nm) of a stoichiometric target, on top of a 85 nm buffer adaptation layer of epitaxial strontium titanate (STO) formed on MgO. In the case of sample LEY4809d, the STO layer was covered by twenty double layers (6 nm YBCO/7 nm STO) before the active film was deposited [15]. Alternatively, we could use films dc-sputtered from multiple targets fabricated at CEA-Grenoble, or electron-gun deposited from a stoichiometric target (LL109-N) at CSNSM-Orsay. When available, electron microscopic observation revealed the crystalline state of the YBCO surface, featuring twins on a typical scale of 0.3 micrometers. In all cases, the bridge pattern (5 to 40 μm wide; two or four terminals) was obtained by standard photolithography plus ion beam etching.

Gold contact pads were formed at 250°C, under oxygen pressure, on the sputter-etched material, by using in each case the most suitable method (RF sputtering or

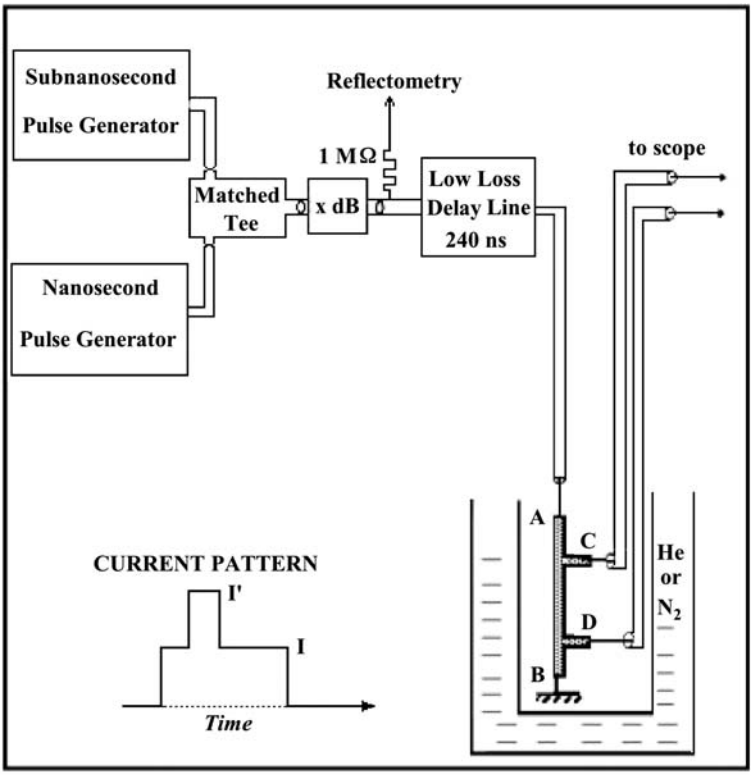

Fig. 2 Experimental apparatus. One, or two, pulse generators, connected through calibrated resistive attenuators (x dB, in steps of 0.1 dB) deliver rectangular pulses on a 50-ohm line. The sample is cooled by nitrogen, or helium. It can be directly immersed in the liquid, or enclosed in an evacuated copper cell

Joule evaporation). Since the experiment may involve large currents, up to 250 mA at low temperature (TO-34; T704a3), a straightforward interpretation of the measurements relies heavily on the quality of the electrical contacts. These procedures resulted in contact resistances R_0 of the order of 30 mΩ, at least in the first low-temperature run. This value could degrade to 50 mΩ or more after a dozen runs. Samples having $R_0 \geq 150$ mΩ were either repaired or discarded.

Figure 2 is a sketch of the experimental apparatus. Single rectangular current steps, or more complicated waveforms, of duration up to about 400 ns, are delivered by one or two pulse generators (analog + digital) to a coaxial line of wave impedance $Z = 50$ ohms. A 240-ns air delay line allows monitoring the input and the reflected pulses separated in time, thus probing a two-terminal device by reflectometry, for use when the lateral probes are not available. The analog source is capable of a finer control of I_c, defined as the current producing the longest observable PSC delay time. Let us note that, although individual currents are known to no better than ±1%, current ratios, such as I/I_c can be certified to about ten times better accuracy, thanks to the use calibrated coaxial attenuators.

In order to clearly distinguish the various modes of dissipation (VF, PSC, HS), it is essential to achieve satisfactorily the condition of constant-current bias. What is easily obtained as long as the superconducting bridge has negligible impedance, becomes problematic when resistance sets in. A simple analysis, neglecting inductances and attenuation along the cables, shows that the time-dependent current I through the strip is related to the input voltage V_i by the relation $I = (2V_\mathrm{i} - V)/Z$, where V is the instantaneous voltage measured at a lateral probe (provided the dissipative center occurs beyond that particular probe). As we will soon see, the rising signal of an expanding HS becomes visibly sublinear beyond a sample resistance V/I of about 3 Ω, and eventually goes to saturation typically around 8 Ω. That might lead to confusion with a PSC voltage, unless these numbers are taken into account. Due to their rather high resistivity, YBCO bridges are likely to show this behavior, and only the initial development of a HS may be significant. An alternative was to insert a (compact) impedance bridge close to the sample to increase the effective series resistance. Similarly, the voltage probes were occasionally linked to their respective coaxial cables *via* a 150-ohm resistor.

Experiments were performed from 1 K to about 85 K, with standard temperature controls and cryostatic systems, including pumped liquid helium and pumped liquid nitrogen. The size of the substrates, and their high thermal conductivity, insure that the "bath temperature" T_b is unaffected during a submicrosecond electrical pulse.

4 Current-Induced VF, PSCS, HSS and the I–T Diagram

Under pulsed excitation, the delay time t_d which precedes the PSC or HS responses sufficiently distinguishes these modes from the flux-flow (VF) regime, since there is no delay for the VF resistance except, possibly, on the scale of τ_0. The VF resistance illustrates the two-dimensional character of YBCO films ($w \gg \xi$), and usually sets in at elevated temperatures, finally exclusively dominating the response within about 5 K of T_c. The inset of Fig. 3 shows the VF voltage response in microbridge T704a3 fed with current-controlled step pulses. The depinning threshold at 80 K is $I_\mathrm{VF} \sim$ 12.3 mA, corresponding to a current density of $J = 2 \times 10^6$ A/cm^2. After a rounded initial rise, the voltage *versus* current graph displays a linear behaviour consistent with a fixed concentration of vortex tubes driven by the Lorentz force.

At a lower temperature (73 K), the vortex flow signal (Fig. 4a; trace α), still present, shows a slower saturation, as a consequence of the reduced VF resistivity and resultant increased penetration time of the magnetic induction. More striking is the delayed appearance, for a (depairing) current I_c, of a phase-slip center, denoted PSC1, appearing as a step-voltage on top of the VF signal (trace β). It is characterized by a delay time t_d rapidly decreasing as the intensity of the drive current increases. If one identifies the current (63.5 mA) giving the longest observable delay (350 ns here) as the critical one, it corresponds to a critical density $J_\mathrm{c} = 10.5$ MA/cm^2, to be compared with $J_\mathrm{VF} = 5.85$ MA/cm^2 for the depinning density at 73 K. For 67 mA (trace γ), the delay of PSC1 is reduced and a second PSC, denoted PSC2, has been nucleated. Some explanation of the waveshapes at early times ($\sim$ 50 ns) is needed:

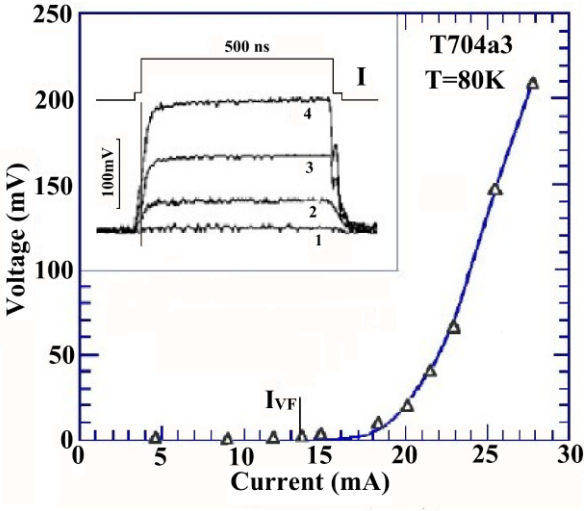

Fig. 3 (Color online) Voltage *vs.* current plot showing vortex creep, followed by linear vortex flow, in zero applied magnetic field. *Inset*: VF voltage *vs.* time for several current intensities: 12.3, 15.1 20.5 and 27.7 mA. The non-strictly equal durations of the two step pulses added entail no material consequence

the contact to ground of the sample became loose and it had to be connected externally, *via* a 1-m cable. This caused some initial ringing, which should not affect measurements performed at long times (several 10^{-7} s).

By subtraction of the VF voltage (extrapolated along the dashed lines in traces b and c), one can extract the PSC voltages ΔV_1 and ΔV_2, and plot the quantities ΔV_1 and $\Delta V_1 + \Delta V_2$ (Fig. 4b) as a function of the real current $I = (V_i + V_r)/Z_0$, where V_i and V_r are respectively the incident and reflected voltages measured by reflectometry at time ≈ 350 ns. The linear dependences of both functions upon the current are manifest, as well as the existence of an excess current $I_S = 53.5$ mA $\approx 0.8 I_{c1}$ (73 K). The mean differential resistance of PSC1 and PSC2, $R_u \sim 4\Omega$, leads to a quasiparticle diffusion length $\Lambda = wbR_u/2\rho \approx 2$ μm. It is not in severe disagreement with $\Lambda = v_F(\tau_c \tau_R/2)^{1/2} \sim 0.9$ μm, that can be derived from the values $\tau_c(73\ \text{K}) = 0.3$ ps, taken from Ref. [13], and $\tau_{in}(73\ \text{K}) = 100$ ps taken from Ref. [14].

For a larger current intensity (≈ 68.5 mA) at the same bath temperature, the voltage response becomes too large to fit in the framework of Fig. 4a. While the delay is reduced to a non-observable value, the response increases quasi-linearly with the time, in the manner expected from an expanding HS. Then it bends down as the resistance of the microbridge becomes non-negligible compared to the characteristic impedance of the line. (At $V/I = 5$ ohms, the current intensity may have dropped by 5% of its initial value).

Reducing the temperature ($T_b = 65$ K in Fig. 5) not only inhibits the vortex flow, but it also increases I_c beyond I_h, thereby preventing the possibility of a PSC with a core temperature $T_m < T_c$, because of excessive Joule heating. Therefore, a hot spot bursts from the transient PSC state $\{T_b, I_c(T_b)\}$, according to the trajectory leading to $HS_<$ in Fig. 1a. (Multiple hot spots were never observed, even in the transient state). The present graphs with $dV/dt \sim 7.2$ V/μs, yield a HS velocity of growth $U = (wb/2\rho I)(dV/dt) \sim 52.5$ m/s, a result compatible with U_0 estimated at the end of Sect. 2. Finally, we recall that the apparent HS delay time is just the nucleation

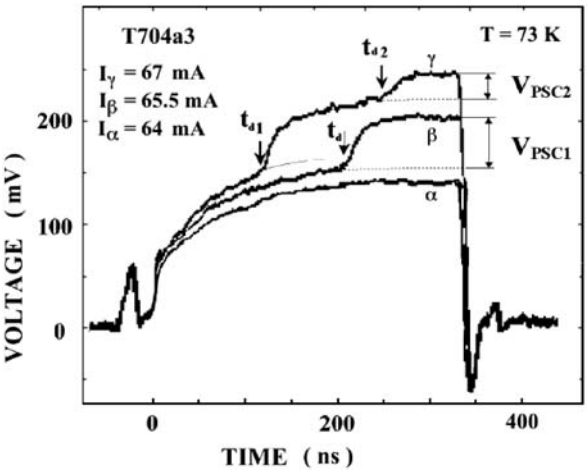

Fig. 4a Voltage signals *vs.* time recorded in sample T704a3 at $T_b = 73$ K, for several current intensities. Traces (α) 64 mA: VF only. (β) 65.5 mA: VF + PSC1. (γ) 67 mA: VF + PSC1 + PSC2. The first ~ 50 ns of the signal have no direct significance (*see text*)

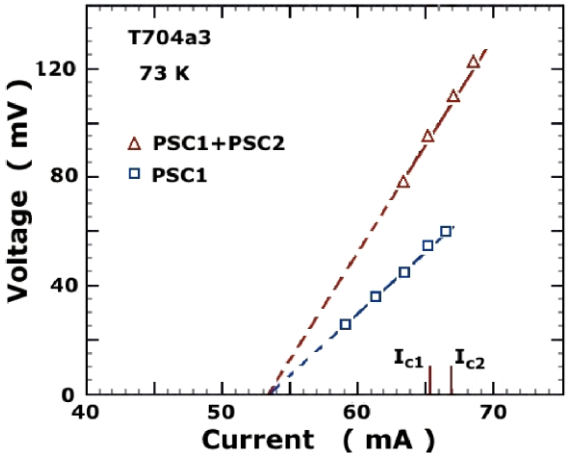

Fig. 4b (Color online) PSC voltages as functions of the instantaneous current measured at time 350 ns, except for PSC1 of trace γ, taken just prior to PC2

time of the transient PSC necessary for initiating the HS state, if YBCO filaments are to behave like Nb filaments [6].

Turning to considerations of heating, the linearity of the two I–V plots in Fig. 4b is somewhat surprising. A rise of a few kelvins from $T_b = 73$ K should produce a small increase of the resistivity, a significant reduction of I_c, and therefore of I_S, causing an increase in the dissipative [1] current $(I - I_S)$, with a proportional effect on V. The other consequence is a reduction of the diffusion length Λ, through the variations of τ_c and τ_{in}, causing a counter effect on V. A detailed study of these effects is beyond the scope of this paper.

Results available from sample T704a3 for I_c and I_h, and also for the VF depinning current I_{VF}, are plotted in Fig. 6 as a function of T_b above 64 K. (At that temperature, the flux flow signal is practically inhibited. *See* Fig. 5.) Although $I_c(T)$ and $I_h(T)$ are virtually defined without limits in temperature, some portions of their I–T diagram have escaped investigation for two reasons: (a) at low T, to avoid excessive

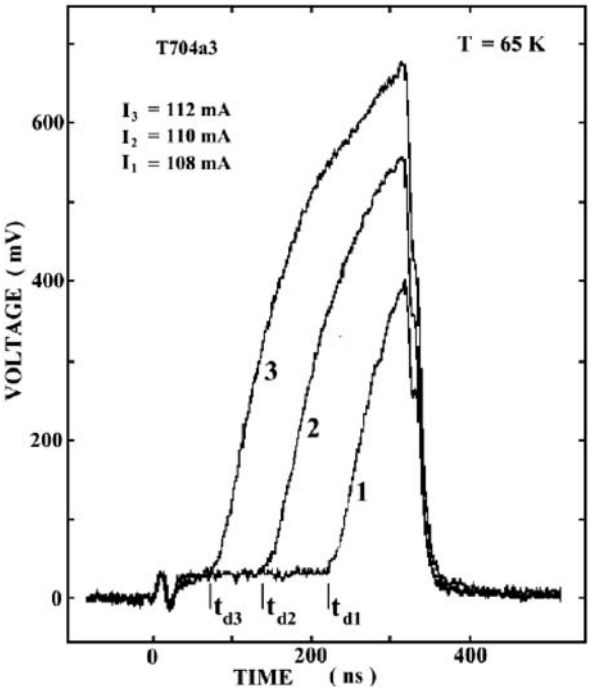

Fig. 5 HS voltage signals at $T_b < T^*$ in strip T704a3 for three current intensities measured in the $R = 0$ state of the device. Note the well-defined delay times, and the initial linear growth of the signals. The subsequent bending is due to imperfect control of the current supply

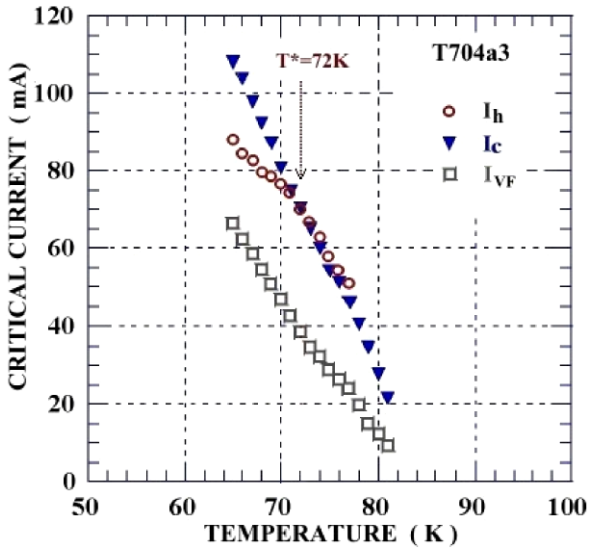

Fig. 6 (Color online) Plot *vs.* temperature of the 3 threshold currents I_c, I_h, and I_{VF}, measured in YBCO sample T704a3 from 64 to 82 K. Below 65 K, the VF voltage disappears. Above 80 K, it far exceeds the PSC signal

dissipation and (b) near T_c, because of the dominance of the VF response over the PSC and HS signals. Throughout the range 65 K to 81.5 K, I_{VF} happens to be about 60% of I_c. Below T^*, I_h was obtained following the method pictured in Fig. 1b, by using a two-step excitation. Let us note that, despite the apparent proximity of

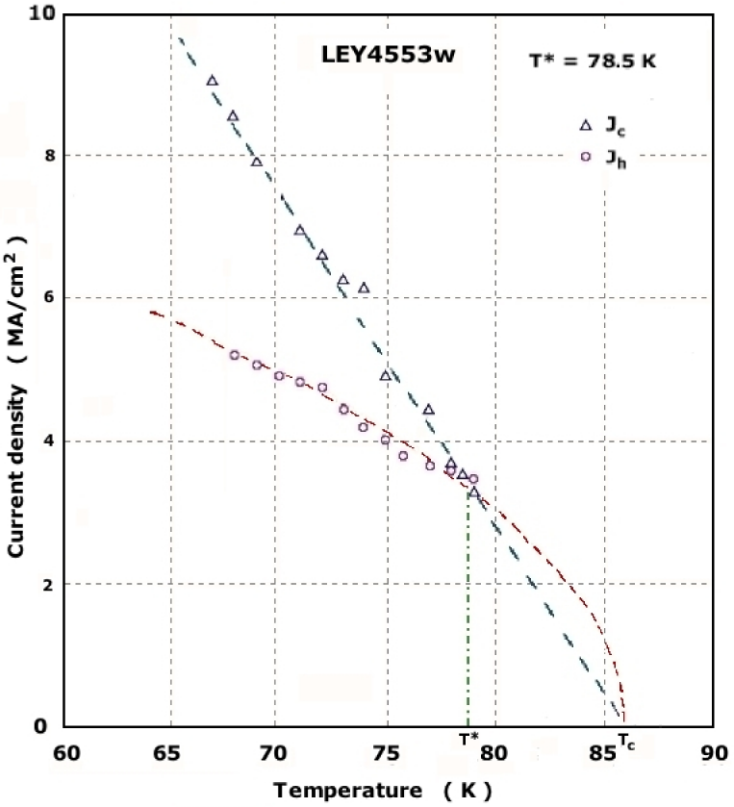

Fig. 7a (Color online) Plots of $J_c(T)$ and $J_h(T_b)$ in YBCO strip 4553w ($b = 120$ nm). The fitting curves (*dashed*) are, respectively, linear for J_c, and parabolic for J_h

their respective plots, $I_c(T)$ and $I_h(T)$ have a well-defined intersection ($T^* = 72$ K; $I^* = 70.8$ mA). The sharpness of the transition from one regime to the other can be appreciated from the contrast between the $T < T^*$ domain (HS only, Fig. 5) and the PSC domain appearing at $T_b = 73$ K (Fig. 4a), only 1 K above T^*.

Similar I–T diagrams were drawn for samples LEY4553w (Fig. 7a) and T704b2 (Fig. 7b). In both cases, $I_c(T)$ is well fit by a straight line extrapolating to $\{I = 0; T = T_c\}$. On the other hand, the HS threshold current $I_h(T)$ can be represented by a parabola having its vertex at T_c.

The principal characteristics of the samples and results relative to their I–T diagrams are collected in Table 1. Quantities directly measured (heavy print) are distinguished from those computed (in parentheses), such as the critical current densities J_c that were extrapolated according to

$$J_c(t) = J_{c0}(1 + t^2)^{1/2}(1 - t^2) \tag{3}$$

a formula where the monomial $(1 - t^2)^{3/2}$ of (15) of [8] has been adapted for *wide* strips ($w > \lambda$).

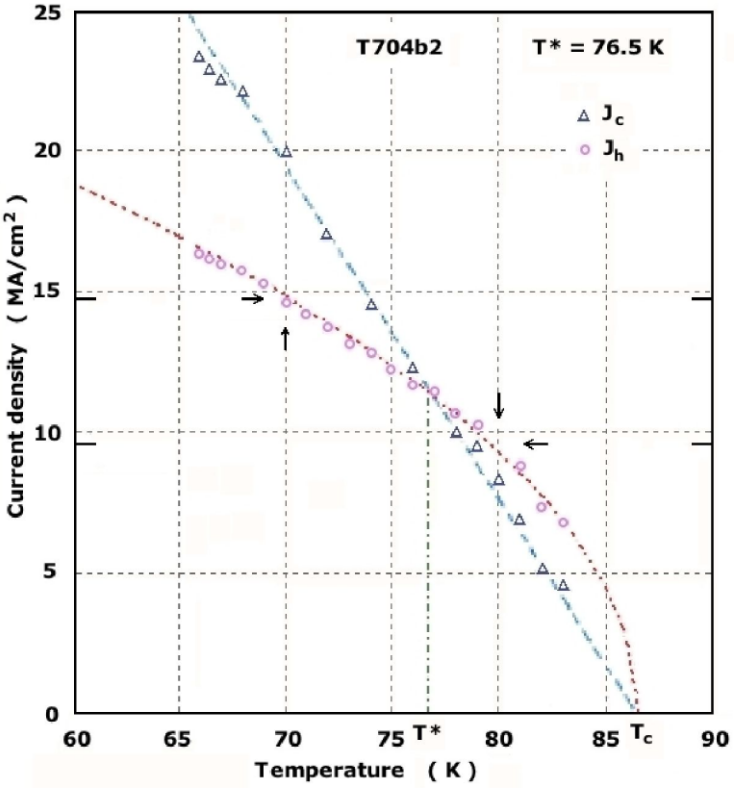

Fig. 7b (Color online) Similar plot in T704b2 ($b = 30$ nm). The values $J_h = 9.05$ and 14.5 MA/cm^2 marked by arrows for $T_b = 80$ and 70 K respectively, are theoretical predictions from (2), with τ deduced from delay times (*see* Appendix)

Similarly, the J_hs are either directly measured, or derived from (2′) that relates I_h to the enthalpy $h(T)$ of YBCO and to the thermal time constant τ taken as $\tau/\text{ps} = 75$ (b/nm) for the filaments deposited on MgO substrates, or otherwise determined from an analysis of the PSC delay times (*see Appendix*). PSCs were obtained in all the samples mentioned. The line "Low-T PSC" specifies whether these PSCs could be observed simply below T^*, as it will be developed in the next section, or even observed at helium temperatures in low-J_c filaments (Sect. 6).

5 Return from a Hot Spot State

Once a HS state has been established, it can be made to retreat by reducing the current. Let us again consider our previous excitation scheme (Fig. 1a, b) consisting of a brief intense pulse I' to initiate a hot spot HS', followed by a longer "return" current pulse, whose magnitude I determines a variety of responses from the filament. In Fig. 8a, taken at $T_b < T^*$, trace 4 shows an increasing HS signal, that grows from

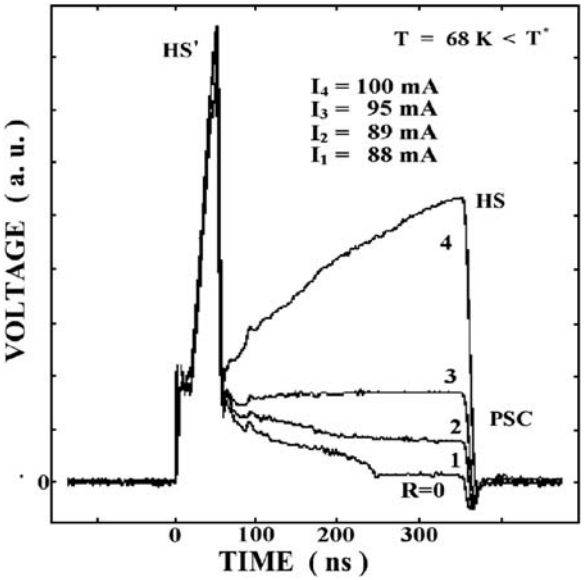

Fig. 8a Return from HS' at $T_b = 68$ K in microbridge T704b2. Return currents $I \geq 95$ mA support a HS, either growing (trace 4), or fixed in length (trace 3). A PSC plateau (trace 2) is reached for $89\ mA \leq I < 95$ mA. Trace 1 shows the HS recession and collapse. (The baseline $R = 0$ corresponds to the voltage drop in contacting pads and wires). Vertical sensitivities are adapted for each trace so as to normalize the HS' signal

the remnants of HS' after the end of the I' pulse. For smaller values of I, the positive slope diminishes until, for $I = 95$ mA, a quasi-plateau is obtained (trace 3). That limiting value of the current is, as in Fig. 1b, the working definition of the thermal threshold current $I_h(T_b)$. By continuity, the expected response to a current $I < I_h(T_b)$ should be a HS receding linearly towards zero. This is not the case. Instead, from 95 mA down to the limiting current called $I_{lim}(T_b) = 89$ mA (trace 2), there is a range of I producing steady voltages that, we believe, *are PSC signatures*. Finally, for $I < I_{lim}(T_b)$, the voltage waveform (trace 1) has the character of a receding HS, with a more or less linear descent, terminated by a sudden collapse once the HS extension has shrunk to twice the thermal healing length η. From the voltage drop ΔV of about 20 mV, one finds here a value of $2\eta \approx 200$ nm, not far from the prediction $2\eta = 2\sqrt{D_{th}\tau} = 165$ nm).

In support of the PSC interpretation, the long-term (or final) voltage was plotted *vs.* I (Fig. 8b) in the above range 89 to 95 mA. Its linear variation, reminiscent of that of Fig. 4b, implies a differential resistance $R_u = 8.5\ \Omega$, corresponding to $\Lambda = 4.5$ μm. If we suppose that the minimum PSC current $I_{lim} = 89$ mA is equal to the critical current at the (unknown) PSC core temperature T_m, likely to be shifted up from the bath temperature $T_b = 68$ K, it is $T(I_c = 89\ \text{mA}) = 74$ K from inspection of the experimental (I, T) diagram of sample 4809d (Fig. 7b).

As a cross check, it is interesting to make an evaluation of the temperatures reached inside a PSC or a HS. In the HS case, the temperature profile is relatively flat near the centre as soon as the normal zone exceeds a few η's, so that the longitudinal (along the strip) heat loss can be neglected. Then the central temperature T_M can be computed using the condition: Dissipation rate per unit volume = Transfer rate to the substrate, namely

$$\rho J^2 = \rho(T_M) I^2 / w^2 b^2 = \tau^{-1} \Delta h(T_b \rightarrow T_M) \tag{4}$$

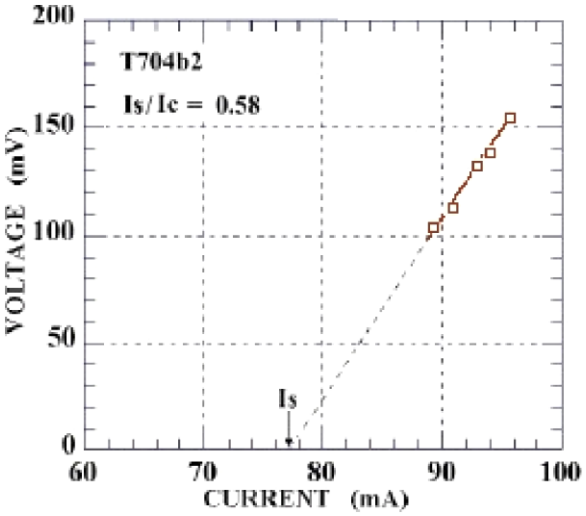

Fig. 8b (Color online) Plot of the plateau voltage V as a function of the return current I in the PSC domain (sample T704b2). The critical current I_c (68 K) = 133 mA is far out of frame

by adaptation of (2′). The PSC temperature profile is not as flat as the HS one, but the low thermal diffusivity of YBaCuO again allows neglecting the longitudinal heat conduction for the calculation of the PSC core temperature T_m. Now, the dissipation $\rho I(I - I_S)/w^2b^2$ per unit volume of the filament replaces $\rho I^2/w^2b^2$ of the normal state, so that T_m is given by

$$V I \tau = 2\Lambda wbC[T_m - T_b] \tag{5}$$

where 2Λ is a simplification of the effective length $(2\Lambda + 2\eta)$ of Ref. [16].

Being the border between the HS and the PSC behaviors, the PSC upper bound, (95 mA for sample T704b2 at $T_b = 68$ K), should be compatible with both these states. Equation (4) with $\rho(100\ \text{K}) = 70.5\ \mu\Omega\,\text{cm}$ and $\tau(\text{T704b2}) = 2.25$ ns leads to $\Delta h = 40\ \text{J cm}^{-3}$ and therefore $T_M = 103$ K for a steady HS. On the PSC side, the same intensity produces a voltage $V = 156$ mV. According to (5), the temperature excursion is only ~ 6.5 K, which maintains T_m safely in the superconducting state.

At the lower end of the PSC range, $I_{min} = 89$ mA and $V_{PSC} = 105$ mV, a similar calculation yields $T_m - T_b = 4.1$ K, and therefore $T_m \approx 72$ K, that is to be compared with the result 89 mA $= I_c(74\ \text{K})$ obtained above. This agreement to better than order-of-magnitude reinforces the PSC assumption, and the measurement of $I_{lim}(T_b)$, coupled with a $T \leftrightarrow I_c$ plot, leads to a reasonable determination of a PSC core temperature. (In the normal state, (4) would lead to $T_M \sim 100$ K, far out of the superconducting range.)

A simplified view of the PSC generation process is as follows: as soon as I is reduced to below $I_h(T_b)$, the hot spot undergoes a regression in T_M and in size (down to 2η) until its own center sinks abruptly below T_c. For a short time, the local I_c is vanishingly small, so that I is largely overcritical, and a PSC-type process can start. It will settle at a central temperature $T_m(I) > T_b$ if the electrical dissipation $V.I$ is able to prevent the reentry into the $R = 0$ state.

It is interesting to map these various behaviours on an I–T diagram, such as Fig. 9, specialized to the case $T_b < T^*$, with the points U and L marking the relevant val-

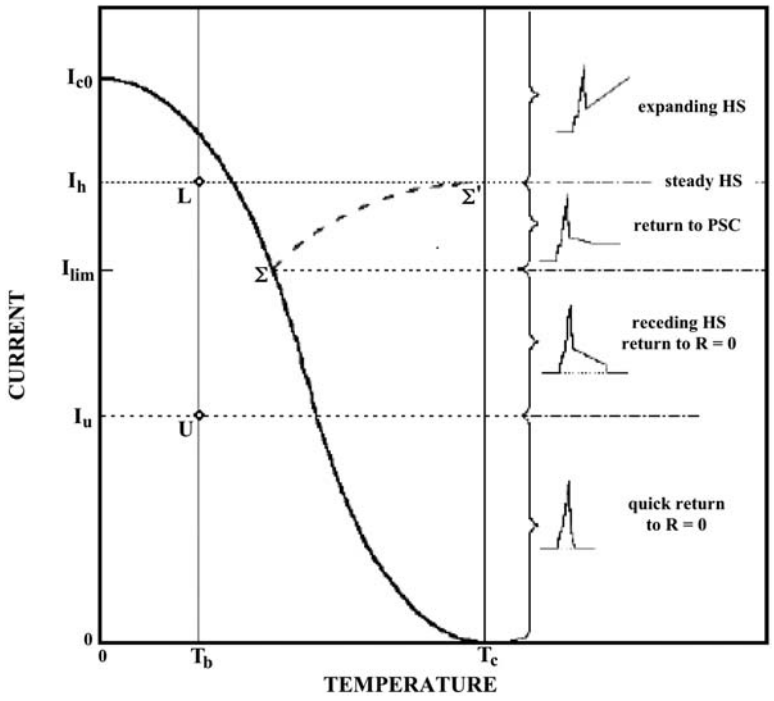

Fig. 9 I–T diagram used to picture the evolution of a normal region suddenly fed with a lower "return" current I (*refer to* Fig. 1b), whose intensity determines the type of response (schematized on the *right*)

ues of $I_u(T_b)$ and $I_h(T_b)$ respectively. For $I > I_h(T_b)$, the response is an expanding HS. In the PSC range $I_{lim}(T_b) < I < I_h(T_b)$, the presumed $I \leftrightarrow T_m$ relation is described by the dotted curve running from (Σ') to its intersection (Σ) with the $I_c(T)$ curve. Continuing with smaller return intensities leads into the domain of the receding HS, provided $I_{lim} > I_u$, a condition fulfilled for trace 1 of Fig. 8a, since there $I_u \sim I_h/\sqrt{2} = 95\ \text{mA}/\sqrt{2} = 67\ \text{mA}$, while I_{lim} is 89 mA. Eventually, below $I_u(T_b)$, at a value of I difficult to point accurately, the entire normal length should resume a non-dissipative state (signal not shown in Fig. 8a) in a time of a few τ's, without any linear descent.

Detailed observations of the same type were made on sample LEY4553w, with similar patterns of temporal response. No qualitative difference showed between $T_b = 77$ K and $T_b = 79$ K, on opposite sides of $T^* = 78.5$ K.

6 PSCs at Low Temperature in Small-J_c Filaments

Any decrease, obtained by design or accidental, of the critical current $J_c(T)$ reduces T^* and extends the natural PSC domain ($T^* < T_b < T_c$) towards low temperature. In the extreme case, summarized by $J'_{c0} < J_{h0}$ (*see* the dashed curve ending at J'_{c0} in Fig. 1), where $J_c(T)$ and $J_h(T)$ do not intersect, there seems to be no lower bound

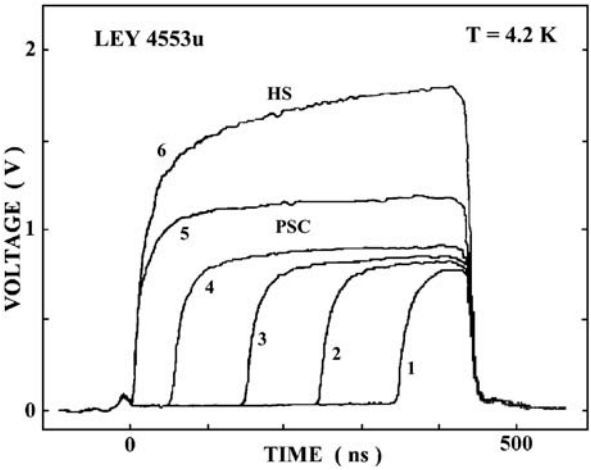

Fig. 10 Low-temperature (4.2 K) voltage response *vs.* time of filament LEY4553u excited by the superposition of a fixed, slowly rising, major pulse, and a fast, finely adjustable pulse. Before t_d, currents (in mA) are successively: 123.45; 124.1; 125.3; 129.7; 148.1; 149.1. PSC nucleation times decrease with the intensity. Note the change of waveshape on the upper trace (*6*), signalling the passage into the HS mode

to the generation of PSCs. Such a situation was not reported for metallic superconductors Al, Sn, In, Nb, Pb, ..., with the exception of low-temperature PSCs reported in niobium [6]. This phenomenon becomes much more accessible in high-T_c materials, where the practical critical current densities are usually far below their theoretical value. A certain amount of control can be exerted on J_{h0}, which behaves like $(\rho b)^{-1/2}$ according to (2). However, a low value of J_{c0} is the key factor, whichever its origin. The recently introduced ultrathin NbN filaments used as single-photon detectors do not seem to satisfy this condition, due to a too large value of their electrical resistivity.

From an experimental point of view, the inequality $I_{c0} < I_{h0}$ should manifest itself at any temperature by the appearance of PSCs, confirmed at the minimum, by a TDGL-compatible nucleation time, a steady voltage under current-controlled drive, and a constant differential resistance. A voltage response increasing linearly with the time, characteristic of a hot spot should appear at some higher value of the current. These features were reported earlier [5] at 4.2 K for the YBCO samples LCZYB-77 and LL109N incorporated in Table 1. Where prohibitively high currents I_{h0} were inaccessible to direct measurement, these were deduced from (2′), and found to obey $J_{c0} < J_{h0}$.

A further demonstration, contrasting the PSC and HS responses at low temperature, is provided in Fig. 10. We see no trace of vortex flow, but rather a sequence of stable nucleation times t_d resulting from closely-spaced values of the input current (values given in the figure caption). Too few t_d measurements could be performed before destruction of the sample to be exploited as in the Appendix. However, the HS threshold current is well defined around 149 mA, and the $I\,(\mathrm{PSC}) \leftrightarrow V\,(\mathrm{PSC})$ graph (not shown) indicates an excess current $I_S \sim 0.65 I_c$, a differential resistance $R_u = 25\ \Omega$, and a quasiparticle diffusion length $\Lambda = 13.2\ \mu\mathrm{m}$ from (5). From the relation between Λ and the microscopic interaction times (Sect. 2), that large length might be due to the low temperature.

While the intrinsic inequality $J_{c0} < J_{h0}$ may result from a particular choice of the sample parameters, the same situation may also result from deterioration of the sample in one of several ways. Surface de-oxygenation of YBCO, destroying the super-

Table 1 Specifications of YBCO strips: thickness b; width w; distance between voltage probes L; number of terminals used [n]; normal state resistivity at 100 K (ρ_{100}), and ratio ρ_{300}/ρ_{100}. Critical temperature T_c. Crossing temperature T^* in the I–T diagram. Pair-breaking current density J_c, in heavy print when measured; bracketed if (extrapolated) through (3). HS threshold density J_{h0} (computed) from (2′), except J_h (4.2 K) directly measured in 4553u (Fig. 10). Same convention for thermal relaxation times τ derived from delay times (Appendix), or alternatively, deduced from (6) (brackets). PSCs observed below T^* by HS quenching (stars), or directly raised at arbitrary low-T (pentagons)

Sample	TO-34a	LCZYB77	LL109-N	LEY4553w	LEY4553u	LEY4809d	T704a3	T704b2
Reference	[20]	[5]	[5]	[9]	[9]	[9]	[21]	[21]
Substrate	MgO	Si	MgO	MgO	MgO	MgO	MgO	MgO
Buffer		YSZ/CeO_2		85 nm STO	85 nm STO	20 bilayers		
b (nm)	30	35	75	120	120	120	30	30
w (μm)	28	10	10	10	10	40	20	20
L (μm) [n]	200 [2]	50 [2]	1000 [4]	500 [4]	500 [4]	500 [4]	200 [4]	200 [4]
ρ_{100} (μΩ/cm)	265	730	125	165	305	190	86.5	70.5
ρ_{300}/ρ_{100}	2.25	2.6	2.8	2.67	2.47	2.71	2.75	2.68
T_c (K)	82	87	89	86	87	88	86	86.5
T^* (K)	None	(74)	None	**78.5**	None	(79.5)	**72**	**76.5**
J_c (77 K) (mA/cm^2)	(1.25)	(3.25)	**1.35**	**3.60**	(2.95)	**1.17**	**7.50**	**11.1**
J_c (4.2 K) (mA/cm^2)	**7.6**	**20.5**	**9.0**	(13.5)	**10.25**	(3.8)	(28)	(40)
J_{h0} (mA/cm^2)	(10.5)	(4.75)	(11.2)	(7.35)	**12.4**	(5.5)	(20.5)	(22.5)
τ (ns)	**2** (2.25)	**5.0**	**6.5** (5.6)	**8.5** (9.0)	(9.0)	**15**	(2.25)	(2.25)
PSC at $T < T^*$				★				★
Low-T PSC	⬠		⬠		⬠			

conductivity over a fraction m of the film thickness, would reduce $I_c(T)$ by a factor 1-m, without changing $I_h(T)$, and therefore would reduce the ratio I_c/I_h in the damaged area, likely to become the sensitive zone. (Hence, the currents I, rather than the densities J, are the relevant quantities.) If the damaged thickness becomes insulating, the result is an increase of the apparent resistivity ρ and a decrease of I_c by a factor of $\sqrt{1-m}$. Let us consider the case of sample LEY4553u, that was prepared in the same run as sample LEY4553w, and was intended to have the same characteristics, but which turned out to be inferior in terms of normal state conductivity (Table 1) and of low-temperature critical current. Its first resistive response at 4.2 K is characteristic of a PSC (Fig. 8), as it should be, in contrast to 4553w which has a HS response (not shown) as soon as $T_b < T^* = 78.5$ K. It seems that the inequality $J_{c0} < J_{h0}$ was induced in this case by ageing.

To summarize this section, resistive structures having the signature of PSCs were observed, at helium temperatures, in three samples (Table 1) characterized by their "low" critical current densities. However, since the superconducting path in YBCO

is made up of a multiplicity of parallel channels, it is not attempted to describe the origin of this property.

7 Conclusion

C-axis oriented $YBa_2Cu_3O_7$ superconducting strips were found to exhibit features characteristic of 1-dimensional transport, namely Phase-Slip Centers and Hot Spots. (The usual vortex flow coexists with these singularities apparently without interference.) The prevalence of one mode over the other is governed solely by the relative values of the macroscopic currents $I_c(T)$ and $I_h(T)$, regardless of the complicated topology of the current lines at the nanometer level in oxide superconductors. Between its center and its borders, a PSC inevitably explores a large span of temperatures, a situation making it difficult to derive detailed information about the electronic lifetimes. On the other hand, the computed local deviations of the film temperature appear quite compatible with the experimental I–T diagrams. Furthermore, one finds an exceptional agreement between the PSC nucleation times and their corresponding TDGL-based theoretical model, even for $T \ll T_c$ (*see* Appendix).

By applying nanosecond pulse techniques, we have shown that a hot spot never arises unless a PSC has been first created, and conversely that a PSC can survive on a substrate cooled well below T^*. This particular hysteretic state is obtained by the quenching of a previously generated hot spot. So, in many respects, $YBa_2Cu_3O_7$ strips behave like conventional metallic superconductors [6]. However, there exist cases (typically filaments having a reduced critical current density) where PSCs can be created in a single step of current at any temperature, a phenomenon singular in the literature of non-equilibrium superconductivity.

Acknowledgements F. Chibane, F.S. Jelila, N'Guyen Hy Hau, and F. Boyer, are acknowledged for their participation at early stages of this work, as well as Profs. Lê Van Hông, Phan Hông Khôi (Institute of Materials Science, HàNôi, ViêtNam), and F.M. Vidal (University of Santiago de Compostella) for their support. This work was contractually supported by ACI DESIQ 2003–2006 with CNRS, and by Convention C-Nano Ile-de-France DSEPU 2007.

Appendix: PSC/HS Delay and Film Cooling Time

Throughout this work, we have made use of a film cooling time τ to evaluate the temperatures reached at the center of either a PSC (T_m) or a HS (T_M). This characteristic time is usually estimated from a phonon-escape theory, or derived from bolometric measurements. However, we use here a quite different determination, *practicable at any temperature in the superconducting state*, based on an analysis of the PSC nucleation time t_d. Our τ is identified with the prefactor τ_d of the Pals and Wolter formula [7]:

$$t_d(I/I_c) = \tau_d \int_0^1 \frac{2f^4 df}{(4/27)(I/I_c)^2 - f^4 + f^6} \tag{6}$$

or $t_d = \tau_d F_{PW}(I/I_c)$ in short. More exactly, we used an improved theory of the nucleation time, due to Tinkham [17], that modifies the numerator of the integral and

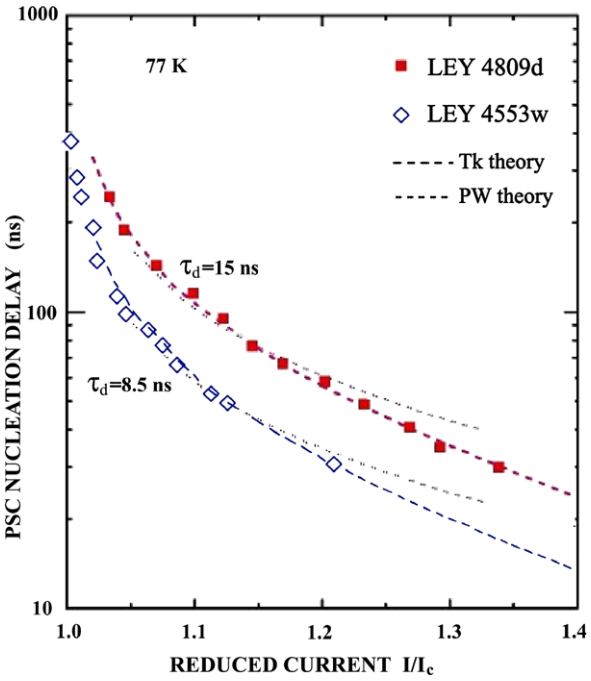

Fig. 11 (Color online) PSC nucleation time *vs.* I/I_c in samples 4553w and 4809d of common thickness (120 nm), but different buffer underlayer. Each plot is compared to the functions F_{PW} and F_{Tk}, with the same prefactor τ_d, considered as a measure of the bolometric response time. F_{Tk} is adapted for $T = 0.9T_c$

its limits. Here the variable f is reminiscent of (the normalized modulus of) the superconducting wave function introduced in the Ginsburg-Landau equation [7]. The predicted t_d can again be factorized as $t_d = \tau_d F_{Tk}$, where F_{Tk} is a function, not only of $I/I_c(T)$, but also explicitly of the parameter T/T_c [6]. Asymptotically equivalent to (6) for $I \to I_c$, it allows dealing with larger I/I_c's and shorter t_ds. Here, we extend it freely to low temperatures, far from T_c, beyond the domain of validity initially claimed [7, 17]. In the original formulation, τ was meant to represent the gap relaxation time, which scales with the short and highly temperature-dependent inelastic electron-phonon time. Instead it was shown, in particular for the case of YBCO filaments [9], that the experimental τ_d is a relatively long (nanoseconds), temperature-independent time, proportional to thickness. Whenever a comparison is possible, τ comes close to the bolometric time τ measured near T_c [18], or above [19], so that it seems legitimate to identify one with the other. Furthermore, owing to the low value of the electron contribution to the total specific heat in YBCO, τ should not differ significantly from the phonon escape time τ_{esc} towards the substrate. Finally, for c-axis oriented YBCO on polished (001) MgO, STO-buffered or not, a number of data [9] can be summarized under the numerical form:

$$\tau \approx \tau_{esc} \approx 75 \text{ (b/nm)ps} \tag{7}$$

over a large span of temperatures. We now give a supplementary example to illustrate the procedure introduced earlier [5]. It concerns two filaments, LEY4553w and LEY4809d, having equal thickness $b = 120$ nm. The essential difference is in the epitaxial buffer multilayer (20 times YBCO + STO), that separates filament LEY4809d

from its STO-covered MgO substrate (*see* Table 1). Figure 11 is a double plot of the PSC nucleation times t_d measured at 77 K in the two samples. The fitting curves are $\tau_d F_{Tk}[T/T_c, I/I_c(T)]$ functions, computed for $T/T_c \approx 77\ \mathrm{K}/T_c \approx 0.9$, with the prefactors $\tau = \tau_d$ as the sole adjustable parameters. One notes the better fits obtained with the function F_{Tk} compared to F_{PW}. If we acknowledge that two YBCO filaments of the LEY series have, by fabrication, similar electrical characteristics, the most relevant difference is to be found in the thermal coupling to their substrates. The multilayer has the effect of roughly doubling the thermal boundary resistance.

The present determination of τ, given by (7), can be subjected to a direct test through (2) that relates the HS threshold current density J_h to the bath temperature. With the choice $p = 2$, $\rho_{100} = 70.5\ \mu\Omega\,\mathrm{cm}$, $C = 1.10\ \mathrm{J/cm^3\,K}$ near T_c and $\tau = 2.25$ ns from (7), applied to sample T704b2, one finds $J_h = 9.05\ \mathrm{MA/cm^2}$ at $T_b = 80$ K, and $J_h = 14.5\ \mathrm{MA/cm^2}$ at $T_b = 70$ K, to be compared with the *directly measured* values in the experimental I–T diagram (Fig. 7b). The agreement is striking, although it might not be as good in samples containing a weak point (signalled by an anomalously high resistivity and a low critical current).

References

1. W.J. Skocpol, M.R. Beasley, M. Tinkham, J. Low Temp. Phys. **16**, 145 (1974)
2. M. Tinkham, *Introduction to Superconductivity*, 2nd edn. (McGraw-Hill, Singapore, 1996), Chap. 11
3. V.M. Dmitriev, I.V. Zomlochevskii, E.V. Kristenko, Physica C (Amst.) **235–240**, 1973 (1994)
4. A. Weber, L. Kramer, J. Low Temp. Phys. **84**, 289 (1991)
5. F.S. Jelila, J.-P. Maneval, F.-R. Ladan, F. Chibane, A. Marie-de-Ficquelmont, L. Méchin, J.-C. Villégier, M. Aprili, J. Lesueur, Phys. Rev. Lett. **81**, 1933 (1998)
6. F.-R. Ladan, K. Harrabi, M. Rosticher, C. Villard, P. Mathieu, J.-P. Maneval, J. Low Temp. Phys. **153**, 103 (2008)
7. J.A. Pals, J. Wolter, Phys. Lett. A **70**, 150 (1979)
8. W.J. Skocpol, M.R. Beasley, M. Tinkham, J. Appl. Phys. **45**, 4054 (1974)
9. K. Harrabi, N. Cheenne, F. Chibane, F. Boyer, F.-R. Ladan, J.-P. Maneval, Supercond. Sci. Technol. **13**, 1222 (2000)
10. A. Junod, D. Eckert, G. Triscone, V.Y. Lee, J. Muller, Physica C **159**, 215 (1989)
11. M. Onuki, T. Fujiyoshi, H. Ohsumi, H. Kubota, T. Hoshino, Physica C **235–240**, 1383 (1994)
12. H. Jiang, Y. Huang, H. How et al., Phys. Rev. Lett. **66**, 1785 (1991)
13. D.A. Bonn, P. Dosanjh, R. Liang, W.N. Hardy, Phys. Rev. B **47**, 11314 (1993)
14. S.G. Doettinger, R.P. Huebener, R. Gerdemann, A. Kühle, S. Anders, T.G. Träuble, J.-C. Villégier, Phys. Rev. Lett. **73**, 1691 (1994)
15. C. Prouteau, J.F. Hamet, B. Mercey, M. Hervieu, B. Raveau, D. Robbes, L. Coudrier, G. Benassayag, Physica C **248**, 108 (1995)
16. A.M. Kadin, W.J. Skocpol, M. Tinkham, J. Low Temp. Phys. **33**, 481 (1978)
17. M. Tinkham, in *Non-Equilibrium Superconductivity, Phonons and Kapitza Boundaries*, ed. by K.E. Gray (Plenum, New York, 1981), pp. 231–262
18. J.P. Maneval, F. Chibane, R.W. Bland, Appl. Phys. Lett. **61**, 339 (1992)
19. M. Nahum, S. Verghese, P.L. Richards, K. Char, Appl. Phys. Lett. **59**, 2034 (1991)
20. F.S. Jelila, J.-C. Villégier, J.-P. Maneval, Physica C **235–240**, 1983 (1994)
21. V.D. Lam, PhD thesis, University of Hànôi, 2004 (unpublished)